

Supplemental material for “Variations in the Biological Pump through the Miocene: Evidence from organic carbon burial in Pacific Ocean sediments”

Mitchell Lyle
Annette Olivarez Lyle

College of Earth, Atmosphere, and Ocean Science, Oregon State University

1.0 INTRODUCTION

This package of supplemental material contains the tables of data we collected for each drill site, the age model, and in the case of Site 574, how we assembled a continuous sediment section from multiple holes (the splice) using image and collected data. For each site we also include tables of other relevant data we have collected, primarily MAR data from XRF scans and discrete carbon analyses.

2.0 Data for Site 574 (04° 12.52'N, 133° 19.81'W)

Site 574 took the most work, since it was drilled in 1985, soon after the hydraulic piston core was first deployed and before techniques for creating a continuous section had been developed. Two holes through the upper sediment column had been drilled and there was an attempt to offset the holes so that core gaps were not aligned. However, there was difficulty because of occasional core disturbance to complete a splice. We used Code for Ocean Drilling Data (CODD, <https://www.codd-home.net/>) software developed by Roy Wilkens to graphically correlate the different holes at the site and join multiple holes into a continuous section (Fig S1). In addition to using GRA wet bulk density data, we also used XRF on the first five cores from Holes 574X (originally 574) and 574A (0-43 m depth in Core Composite below Sea Floor [CCSF] depth scale; Data Table S5). The splice is shown in Figure S1. Core intervals included in the splice are in Table S1, while Table S2 is the table of disturbed intervals within cores.

We established the age model for Site 574 by first using the reported biostratigraphic datum levels (Site 574 Initial Reports, Mayer et al., 1985) to assign an initial age model, and then using the CODD tools to stratigraphically tie the Site 574 CaCO₃ time series to that of nearby Site U1337 (Figure S2) and used the Site 574 equivalent depth in Site U1337 to transfer ages from Site U1337 to Site 574. The resulting age-depth model for Site 574 is shown in Fig S3.

Fig S1: Splice (Continuous sedimentary section assembled from multiple drilled holes) for Site 574. All holes show images of the sediment section extracted from core photographs overlain by XRF CaCO₃ (blue line) and shipboard GRA (gamma ray attenuation density, red line). Hole 574X (originally Hole 574) was drilled to 200 mbsf and a companion hole (Hole 574A) was drilled next to it to overlap uncored intervals between holes. Hole 574C was drilled to late Eocene basement. Yellow lines mark the top of sections included in the splice and lavender lines mark the base of each included section. If sections were just concatenated, the yellow line overlies the lavender one. The splice extends from the surface to just before the initiation of the MCO.

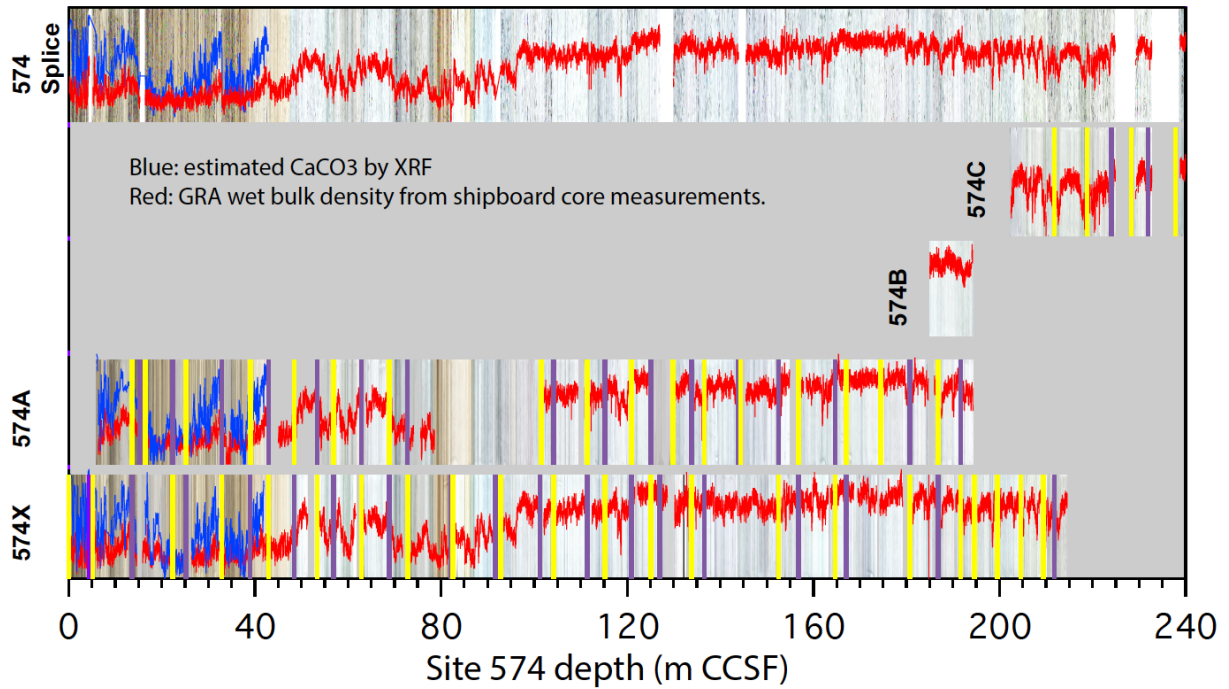


Fig S2: Correlation of Site 574 CaCO_3 time series to that of Site U1337. The black curve (lowest, “stretch site”) is the original CaCO_3 -depth record of the Site 574 splice, while the blue curve is the equivalent CaCO_3 -depth record from Site U1337 (“base site”). CaCO_3 at Site 574 was estimated from (1) XRF, and (2) the high correlation between GRA density and CaCO_3 content in the equatorial Pacific (Mayer, 1991). We used an initial age-depth estimate for Site 574 to assign initial tie points for the two time series and subsequently matched equivalent points on the two CaCO_3 curves using depths. The red curve at the top is Site 574 stretched based on the tie points to an equivalent depth in Site U1337. Once equivalent depths were established, ages could be interpolated from the already dated Site U1337 record. The younger part of Site 574 had a much slower sedimentation rate than that of Site U1337

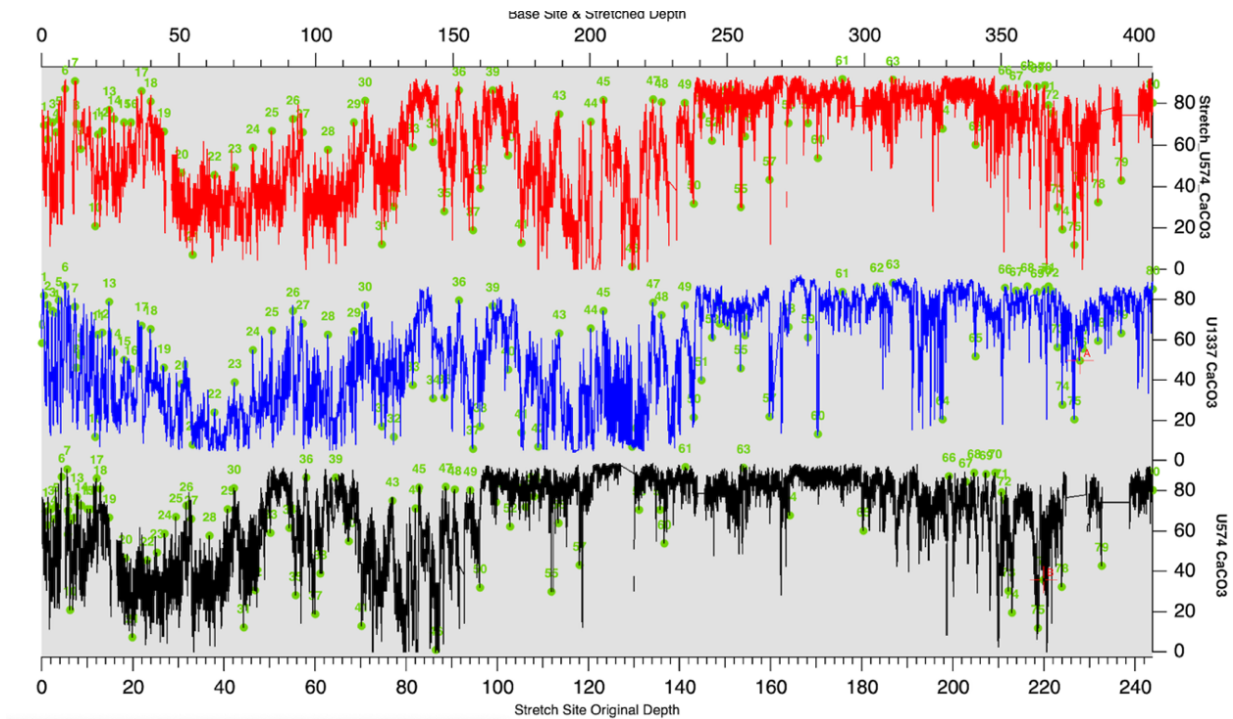
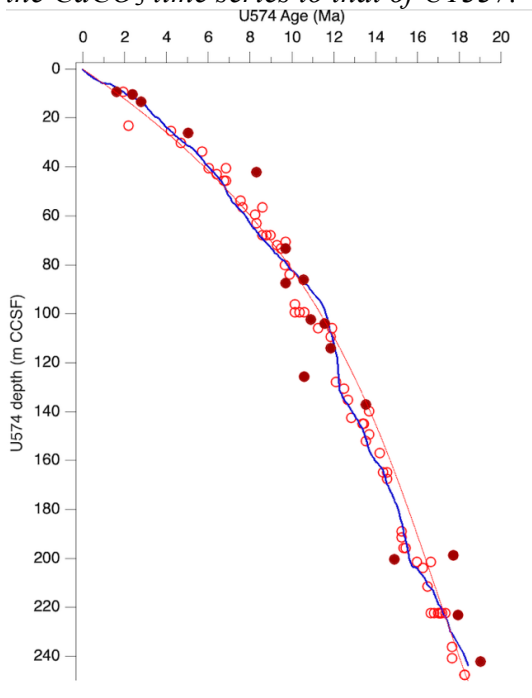


Figure S3: Age-depth relationship for Site 574 resulting from the correlation to U1337. Also shown are the cloud of biostratigraphic datum levels reported for Site 574 in the Initial Reports with ages updated to those in Piela et al. (2012). Filled circles are nannofossil datum levels. Red line is an initial model from the biostratigraphy, while the blue line is after correlation of the CaCO_3 time series to that of U1337.



SUPPLEMENTAL TABLES, Site 574

Table S1: splice interval table for Site 574 (Table of intervals from each hole included in the continuous splice)

Table S2: disturbance interval table for Site 574. These are sections of recovered cores that were disturbed and thus not included in the splice

Table S3: age model for Site 574 on new splice, with estimated CaCO₃% based primarily on GRA density correlated to measured CaCO₃.

Table S4: Site 574 C_{org} wt%, CaCO₃ wt%, depths CSF and CCSF, age, bulk MAR. The carbon measurements are on discrete samples in our lab. Bulk MAR times a species %/100 gives the species MAR in g/cm²/kyr.

Table S5: Site 574A XRF data. Area data are the raw data from the scans, while NMS represents the uncalibrated Normalized Median-Scaled data in % (Lyle et al, 2012).

Table S6: Site 574X XRF data. Area data are the raw data from the scans, while NMS represents the uncalibrated Normalized Median-Scaled data in % (Lyle et al, 2012).

3.0 Data for Site 884 (51 °27.026'N, 168°20.228'E)

Site 884 was drilled on ODP Leg 145 (IR Volume) and is located at the northern end of the Hawaii-Emperor seamount chain. We developed an age model for the site based upon a paleomagnetic reversal sequence measured by the shipboard scientists. We updated magnetochrons from hole 884B to the anomaly ages listed in Westerhold et al. (2020) and built a sedimentation rate curve base on linear sedimentation rates between magnetochron datums. We estimated dry bulk density for MAR calculations based on shipboard physical properties measurements. Table S7 lists the age model, and Table S8 lists the C_{org}/CaCO₃ data for Hole 884B. Since the Site 884 sediments have relatively high C_{org} contents, we included shipboard data (“ship”) with the data measured in our lab (“lab”). We excluded data with >15% CaCO₃ from the shipboard data to avoid errors associated with biases in C_{org} resulting from the process of subtracting CaCO₃ from a total carbon measurement to obtain C_{org}, as was done by ODP at the time of this drilling leg. Bulk MAR was calculated by making a dry bulk density estimate from a correlation between GRA and shipboard dry bulk density measurements.

Figure S4: Age-depth graph for Hole 884B. Depths are in mbsf not composite depth. Sedimentation rates are from linear interpolations between reported magnetic reversals.

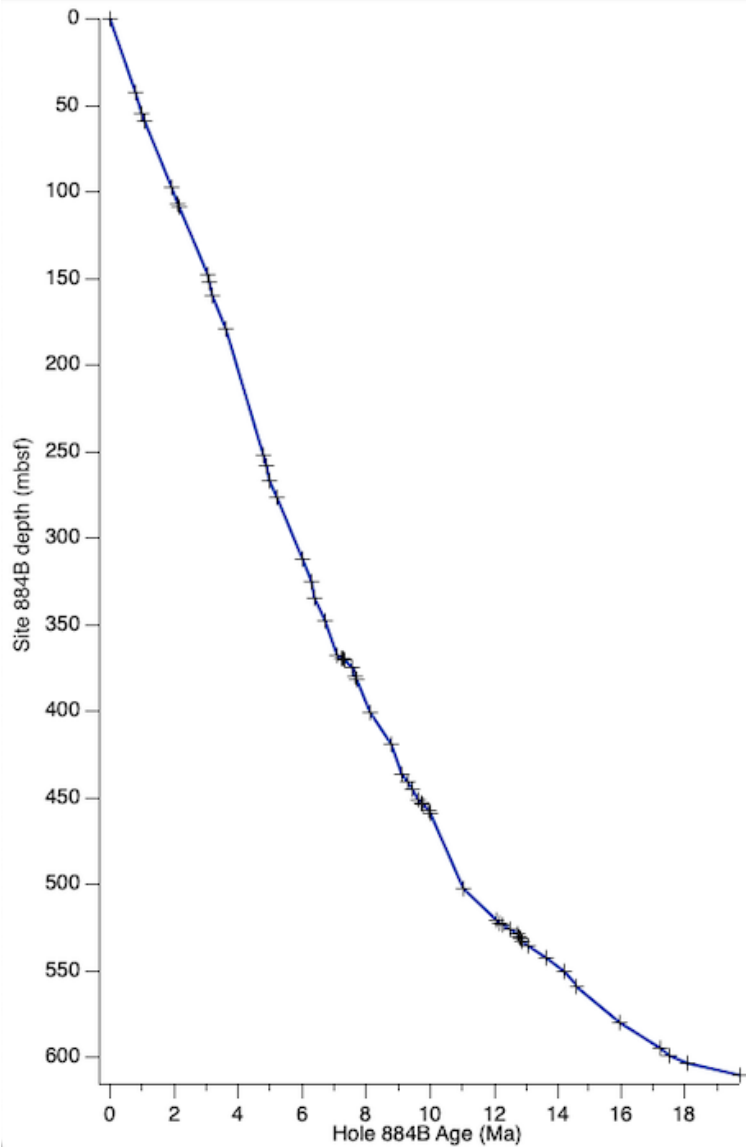
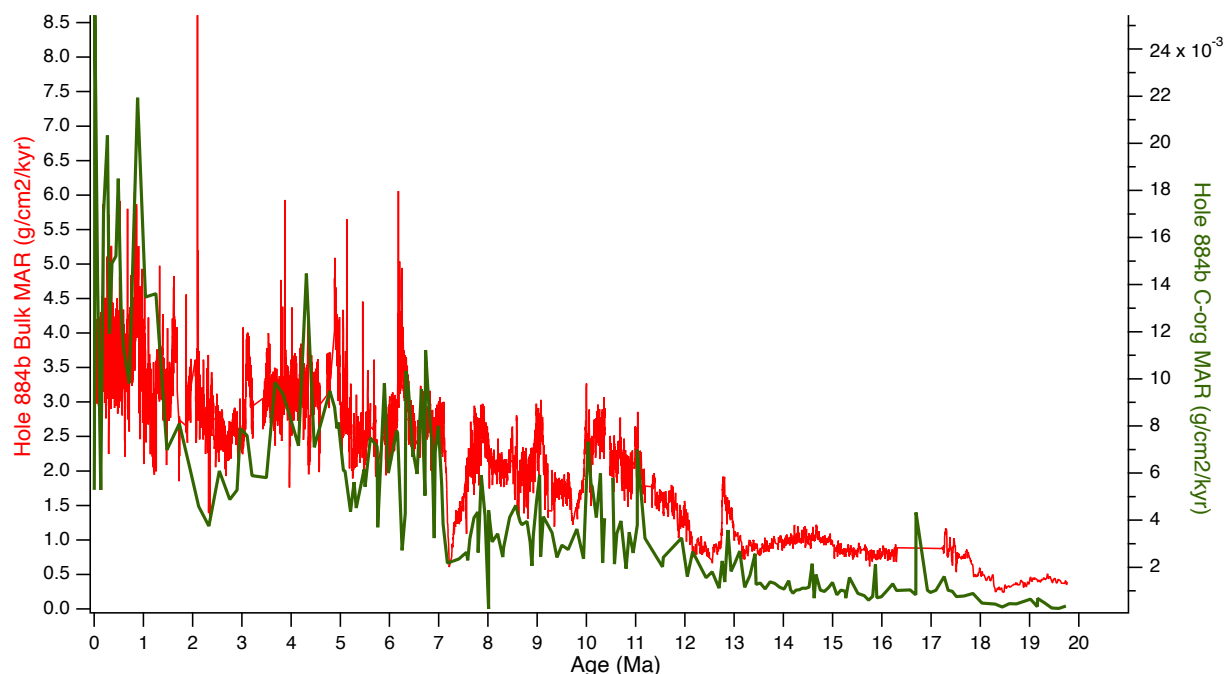


Fig S5: C_{org} MAR (green) and Bulk MAR (red) in Hole 884B from the NW Pacific. The bulk MAR reflects deposition of all sedimentary components. There is a correlation between C_{org} MAR and bulk MAR throughout the record. Site 884 is much more clay rich than the equatorial Pacific which may affect C_{org} preservation.

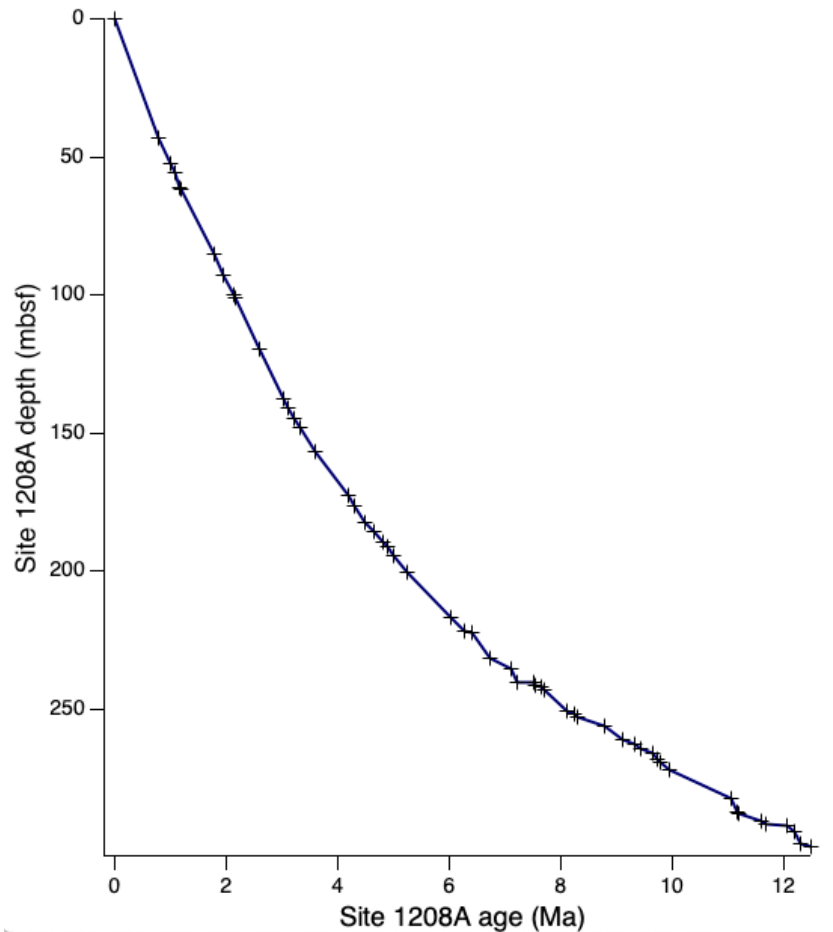


SUPPLEMENTAL TABLES, Site 884
 Table S7: Hole 884B Age-depth table
 Table S8: Hole 884B C_{org} , age, depth, MAR

4.0 Data for Site 1208 (36°7.6301'N, 158°12.0952'E)

Hole 1208A was the only hole drilled at Site 1208 on ODP Leg 198 (Bralower et al., 2002) on Shatsky Rise in the NW Pacific. We collected discrete $CaCO_3$ and C_{org} data from Hole 1208A in support of a project to study paleoceanographic change in the Pacific (e.g., LaRiviere et al, 2012). The sedimentation rate has increased through time since a Paleocene hiatus. We have used Evans (2006, PhD thesis) paleomagnetic data updated to ages from Westerhold et al. (2020) to form the age-depth profile through 12.4 Ma (Table S9). We used linear interpolations of sedimentation rate between paleomagnetic tie points combined with shipboard estimates of bulk density to form bulk MAR. These, multiplied by discrete $CaCO_3$ and C_{org} measurements (Table S10) were used to make MAR profiles

Fig S6 Age-depth graph for Hole 1208A. Depths are in mbsf not composite depth. Sedimentation rates are from linear interpolations between reported magnetic reversals.



SUPPLEMENTAL TABLES, Site 1208

Table S9: Hole 1208A age model

Table S10: Hole 1208A C_{org} , $CaCO_3$, age, depth, MAR

5.0 Data for Site U1337 (3°50.009'N, 123°12.352'W)

Site U1337 had an age model developed by Drury et al. (2017, 2018) and tied to the composite age model developed by Lyle et al. (2019) for Sites 849 and U1338 to 8.1 Ma. Here we correlated stable isotopes for Site U1337 for the 8.1 to 20 Ma section by building an initial age model from biostratigraphy and then correlating the benthic stable isotope records (Tian et al, 2018 Holbourn et al., 2015) from Site U1337 to the CENOGRID Cenozoic isotope splice (Westerhold et al., 2020). The age model was also transferred to the $CaCO_3$ time series to correlate Site U1337 and Site 574. The age model for the $CaCO_3$ time series was also used to transfer ages to the Site U1338 splice from 8.2 to 17.4 Ma.

Figure S7: Oxygen isotope and $CaCO_3$ data for Site U1337. The benthic stable isotope curves (both carbon and oxygen) were used for correlation to establish an age model to 20 Ma (end of isotope data at Site U1337) by correlating to the Westerhold et al (2020) CENOGRID oxygen

isotope age model. The CaCO_3 time series was used to correlate Site 574 to Site U1337. Note that the oxygen isotope curve is plotted with the lightest (warmest) values upward. The lightest part of the record between 17 and 13.8 Ma is the MCO.

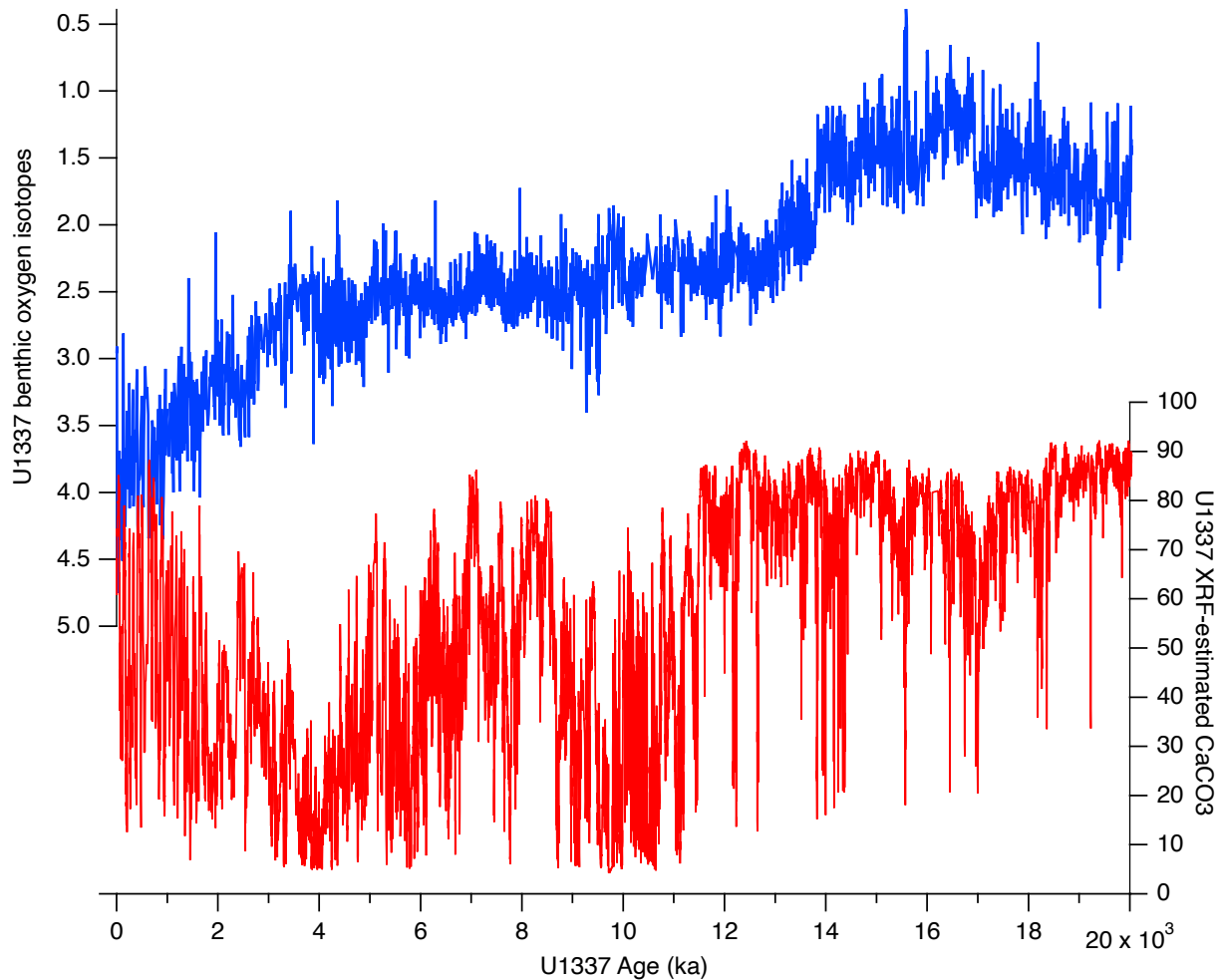


Table S11 lists percentages from XRF estimates and MAR for CaCO_3 , biogenic Si, and BaSO_4 in the sediment. These have been interpolated to 10 kyr intervals from 0 to 8.2 Ma and 20 kyr intervals from 8.2 to 20 Ma. Table S12 lists discrete measurements for C_{org} from our lab, age, bulk MAR, and C_{org} MAR for each point.

SUPPLEMENTAL TABLES, Site U1337

Table S11: Site U1337 age model and XRF estimates of % biogenic CaCO_3 , Bio- SiO_2 , and BaSO_4 , with MAR along the splice, interpolated to 0.01 Ma intervals 0 to 8.16 Ma and 0.02 Ma intervals 8.18 to 20 Ma.

Table S12: U1337 discrete C_{org} measurement data and MAR

6.0 Data for Site U1338 (2°30.469'N, 117°58.178'W)

The age model for the 0-8.1 Ma interval had been developed for Lyle et al. (2019). We added an age model for the 8.1 to 16.7 Ma by correlating The U1338 CaCO_3 record to that of U1337 and then transferring ages from Site U1337 (see Fig S2 for example correlation). Table S13 has all

the C_{org} and $CaCO_3$ data from the discrete analyses plus Ba data extracted from the XRF data at equivalent depths. Bulk MAR was calculated from the sedimentation rates from differentiation of the age-depth curve multiplied by the dry bulk density estimated from the GRA—dry bulk density correlation. Dry bulk density was measured on discrete samples as part of the shipboard physical properties data. Table S14 lists the MAR data for $CaCO_3$, biogenic SiO_2 , $BaSO_4$, and a normative clay estimate. The data were interpolated to 10 kyr spacing from 0 to 8.18 Ma and 20 kyr spacing from 8.2 to 16.7 Ma.

Fig S8: Age-Depth plot for Site U1338. Ages through 8.16 Ma are from Lyle et al. (2019), while ages from 8.18 to 16.7 Ma are from correlations between the $CaCO_3$ time series of U1338 to the dated $CaCO_3$ time series from Site U1337 (Table S11).

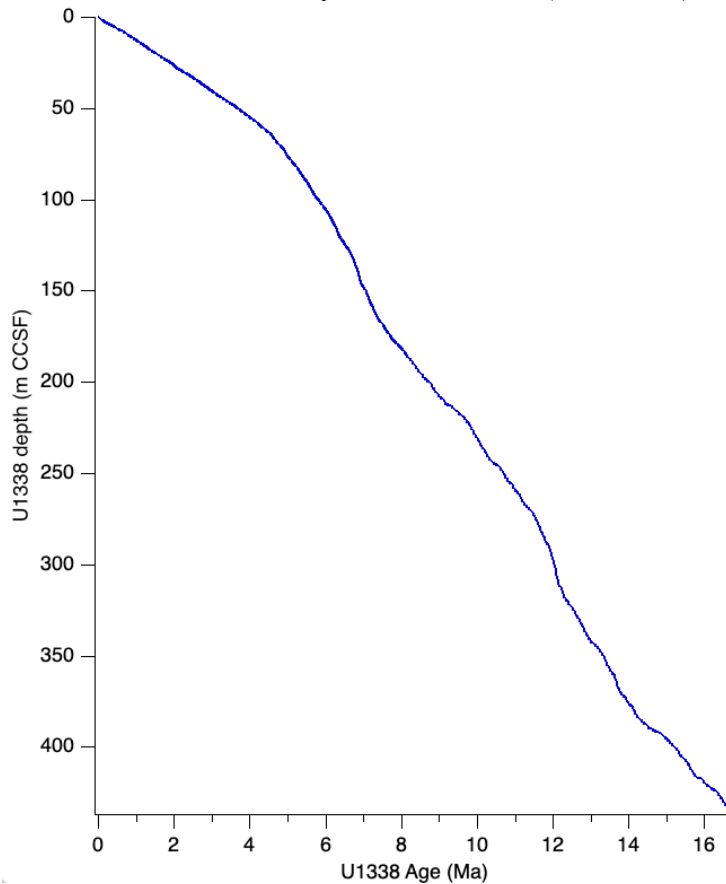
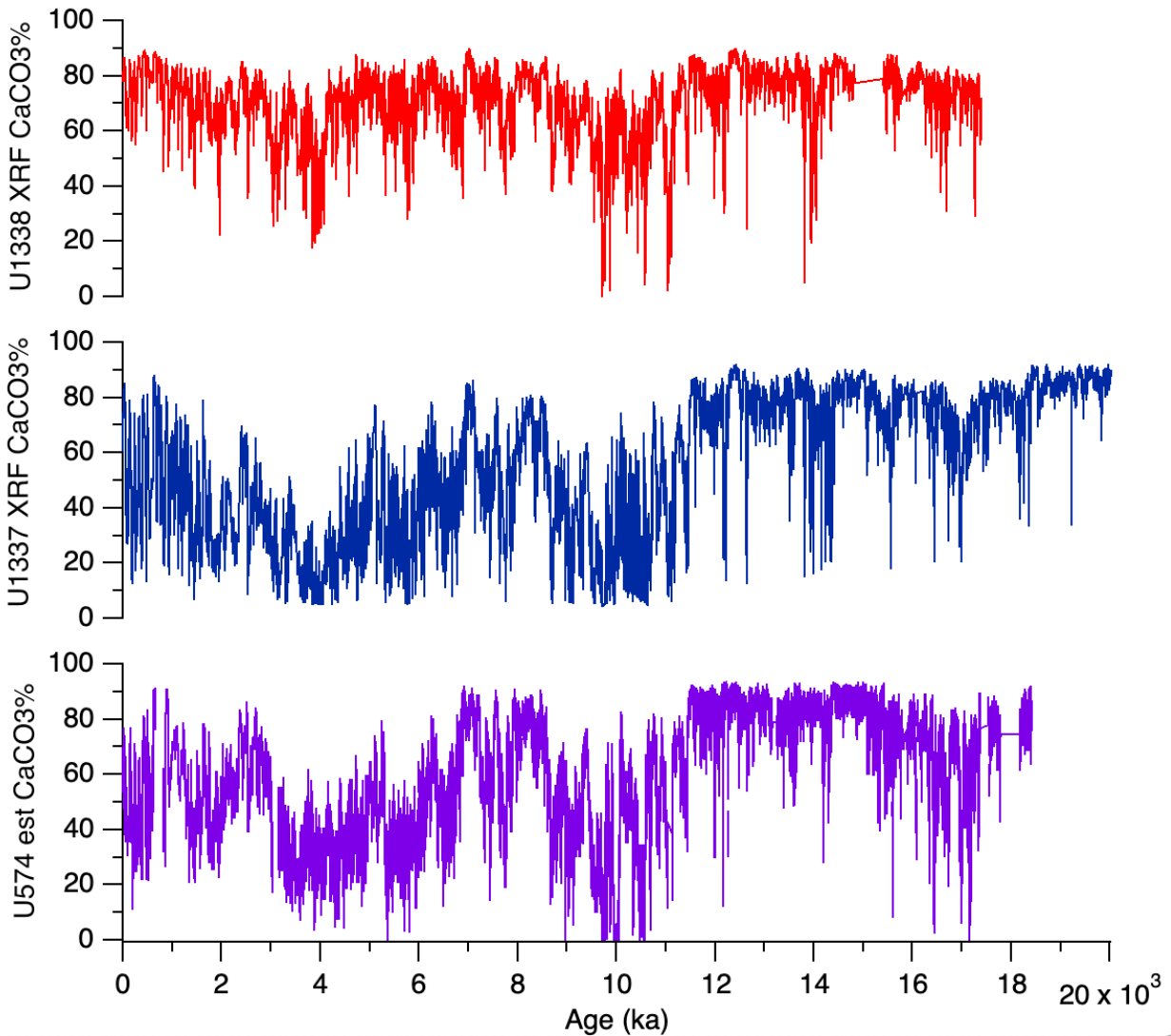


Figure S9: Comparison of $CaCO_3$ profiles for U1338 (top), U1337 (middle), and Site 574 (bottom). Site 574 and U1338 from 8.2 to base of core had ages established by correlation to the $CaCO_3$ profile from Site U1337.



SUPPLEMENTAL TABLES, Site U1338

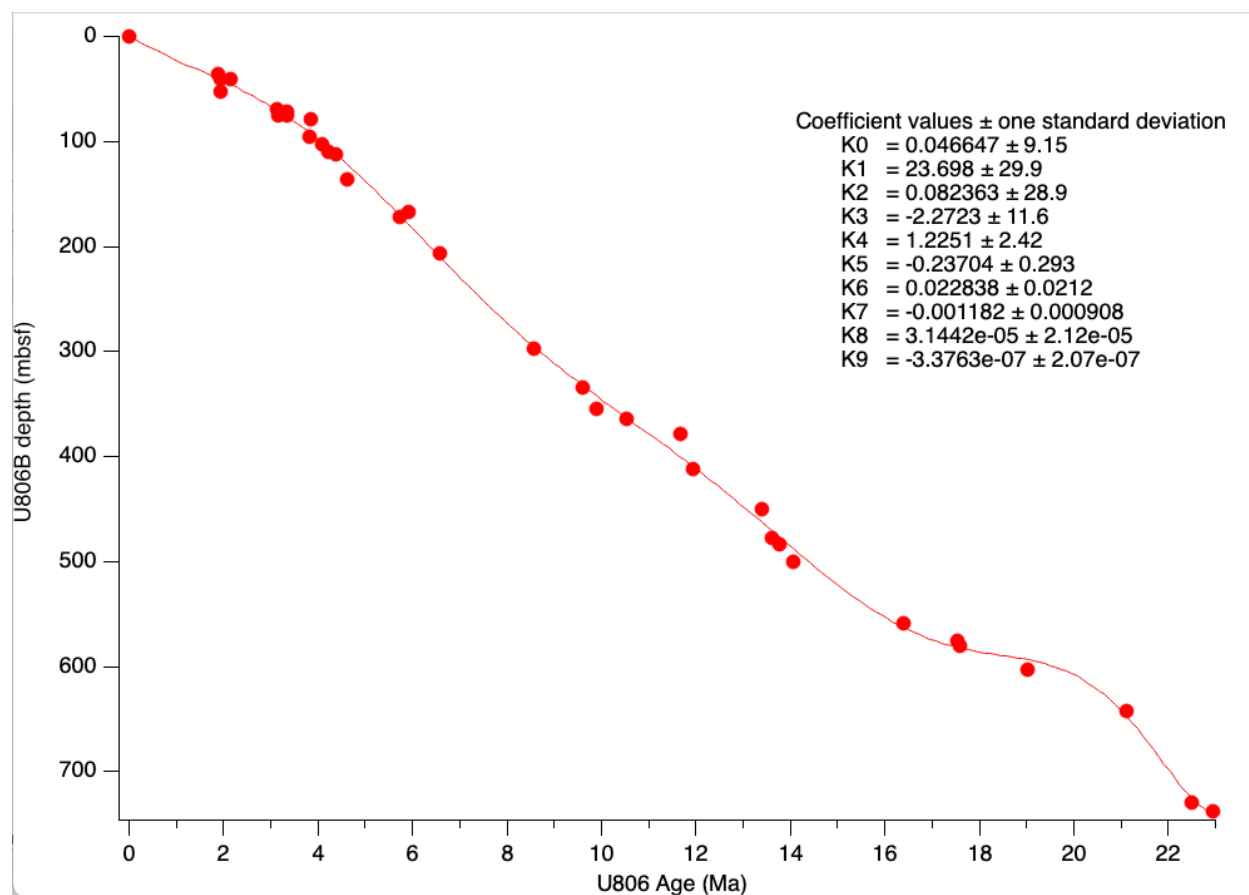
Table S13: U1338 C_{org} and $CaCO_3$ % from discrete analyses with xrf $BaSO_4$ % interpolated to the same positions. Data were then converted to MAR using estimated dry bulk density and sedimentation rate.

Table S14: U1338 XRF and age-depth and MAR based on Lyle et al. (2019) age model to 8.16 Ma and correlation to Site U1337 from 8.18 to 17.4 Ma.

7.0 Data for Site 806 (0°19.11'N, 159°21.68'E)

The data from Stax and Stein (1993) are presented here with an updated age-depth model based on new ages for biostratigraphic datum levels. The update ages are from the Raffi et al (2020) biostratigraphic datum levels. The age-depth data were then fitted with a 9th order polynomial to determine sedimentation rates and dry bulk density was calculated via a dry bulk density-GRA correlation.

Fig S10 age-depth for Hole 806B based on a 9th order polynomial fit through the updated ages for biostratigraphic datum levels measured on ODP Leg 130.



SUPPLEMENTAL TABLES, Site 806

Table S15: Site 806 biostratigraphic data based on shipboard identification and updated ages for datum levels.

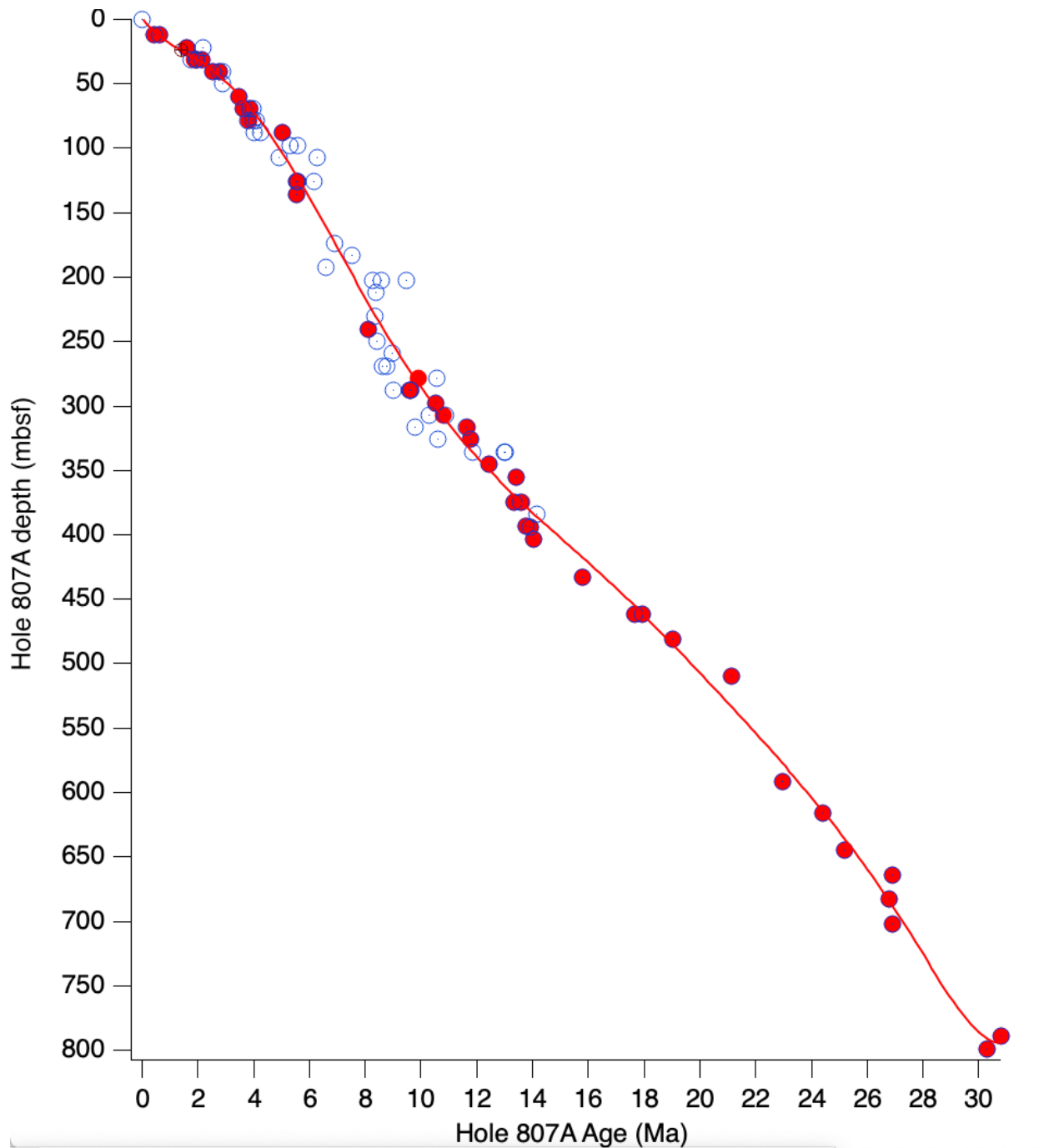
Table S16: Site 806 age model

Table S17: Site 806 discrete Corg analyses from Stax and Stein (1993) with MAR from new age model and estimated dry bulk density from a correlation of dry bulk density to GRA.

4.0 Data for Site 807 (3°36.42'N, 156°37.49'E)

The age-depth curve was derived from a sixth order polynomial fit to the biostratigraphic data updated to Raffi et al (2020, GTS2020) biostratigraphic ages. Because the polynomial went negative at the very top which would produce negative sedimentation rates, I truncated it at 1.393 Ma and substituted a constant average sedimentation rate above, of 11.88 m/Myr.

Fig S11: Age-depth curve for Hole 807A based on a 6th order polynomial fit to the biostratigraphy. Red markers are for calcareous nannofossils and foraminifera, while open blue circles are for radiolaria and diatoms.



SUPPLEMENTAL TABLES, Site 807

Table S18: Site 807 biostratigraphic data from shipboard data and with ages updated from Raffi et al. (2020).

Table S19: Site 807 age model, based on 6th order age model fit through data in Table S18, and a linear age model for the period 0-1.08 Ma.

Table S20: Site 807 discrete organic carbon data from Stax and Stein (1993), with updated ages from Table S18. MAR is based on the age model in Table S19, with dry bulk density estimated from a correlation to GRA

5.0 REFERENCES, SUPPLEMENTAL MATERIAL

Bralower, T. J., Premoli Silva, I., Malone, M. J., and Leg_198_Shipboard_Scientific_Party: Proc. ODP, Init. Repts, Ocean Drilling Program, College Station, TX, doi:10.2973/odp.proc.ir.198.2002, 2002.

Drury, A. J., Westerhold, T., Frederichs, T., Tian, J., Wilkens, R., Channell, J. E. T., Evans, H., John, C. M., Lyle, M., and Röhl, U.: Late Miocene climate and time scale reconciliation: Accurate orbital calibration from a deep-sea perspective, *Earth and Planetary Science Letters*, 475, 254-266, 10.1016/j.epsl.2017.07.038, 2017.

Drury, A. J., Lee, G. P., Gray, W. R., Lyle, M., Westerhold, T., Shevenell, A. E., and John, C. M.: Deciphering the state of the late Miocene to early Pliocene equatorial Pacific, *Paleoceanography and Paleoclimatology*, 33, 246-263, 10.1002/2017PA003245, 2018.

Evans, H. F.: *Magnetic Stratigraphy and Environmental Magnetism of Oceanic Sediments*, Phd thesis, University of Florida, 204 pp., 2006.

Expedition_320/321_Scientists: in: *Proceedings of the Integrated Ocean Drilling Program, 320/321* edited by: Pälike, H., Lyle, M., Nishi, H., Raffi, I., Gamage, K., Klaus, A., and the Expedition_320/321_Scientists, Integrated Ocean Drilling Program Management International, Inc., for the Integrated Ocean Drilling Program, 10.2204/iodp.proc.320321.102.2010, 2010.

Holbourn, A., Kuhnt, W., Kochhann, K. G. D., Andersen, N., and Meier, K. J. S.: Global perturbation of the carbon cycle at the onset of the Miocene Climate Optimum, *Geology*, 43, 123-126, 10.1130/G36317.1, 2015.

LaRiviere, J. P., Ravelo, A. C., Crimmins, A., Dekens, P. S., Ford, H. L., Lyle, M., and Wara, M. W.: Late Miocene decoupling of oceanic warmth and atmospheric carbon dioxide forcing, *Nature*, 486, 97-100. doi: 10.1038/nature11200, 2012.

Lyle, M., Drury, A. J., Tian, J., Wilkens, R., and Westerhold, T.: Late Miocene to Holocene high-resolution eastern equatorial Pacific carbonate records: stratigraphy linked by dissolution and paleoproductivity, *Climate of the Past*, 15, 1715-1739, <https://doi.org/10.5194/cp-15-1715-2019>, 2019.

Mayer, L. A., Theyer, F., and Leg 85 Shipboard Scientific Party: *Initial Reports, 85 U.S. Gov't. Printing Office, Washington*, doi:10.2973/dsdp.proc.85.1985 1985.

Mayer, L. A.: Extraction of high-resolution carbonate data for palaeoclimate reconstruction, *Nature*, 352, 148-150, 1991.

Piela, C., Lyle, M., Marcantonio, F., Baldauf, J., and Olivarez Lyle, A.: Biogenic sedimentation in the equatorial Pacific: Carbon cycling and paleoproduction, 12-24 Ma, *Paleoceanography*, 27, PA2204, 2218 pp, 10.1029/2011PA002236, 2012`.

Raffi I, Wade BS, Pälike H (2020) The Neogene Period (Chapter 29). In *Geological Time Scale 2020*, FM Gradstein, JG Ogg, MD Schmitz, GM Ogg (eds) Volume 2:1141–1215. <https://doi.org/10.1016/B978-0-12-824360-2.00029-2>, 2020.

Stax, R. and Stein, R.: 34. Long-Term Changes In The Accumulation Of Organic Carbon In Neogene Sediments, Ontong Java Plateau, *Proceedings of the Ocean Drilling Program, Scientific Results*, 130, 573-584, 10.2973/odp.proc.sr.130.039.1993, 1993.

Tian, J., Ma, X., Zhou, J., Jiang, X., Lyle, M., Shackford, J. K., and Wilkens, R.: Paleooceanography of the east equatorial Pacific over the past 16 Myr and Pacific-Atlantic comparison: High resolution benthic foraminiferal d18O and d13C records at IODP Site U1337, *Earth and Planetary Science Letters*, 499, 185-196, 10.1016/j.epsl.2018.07.025, 2018.

Westerhold, T., Marwan, N., Drury, A. J., Liebrand, D., Agnini, C., Anagnostou, E., Barnet, J. S. K., Bohaty, S. M., De Vleeschouwer, D., Florindo, F., Frederichs, T., Hodell, D. A., Holbourn, A. E., Kroon, D., Lauretano, V., Littler, K., Lourens, L. J., Lyle, M., Pälike, H., Röhl, U., Tian, J., Wilkens, R. H., Wilson, P. A., and Zachos, J. C.: An astronomically dated record of Earth's climate and its predictability over the last 66 million years, *Science*, 369, 1383-1387, 2020.